Interactive comment on "Calibration of an all-sky camera for obtaining sky radiance at three wavelengths" by R. Román et al.

Author's answer to Anonymous Referee #2

The authors greatly acknowledge the anonymous reviewer (Referee #2) for carefully reading the manuscript and providing constructive comments.

We appreciate the positive comments by Referee #2 claiming that this work contributes to enhance the calibration methods of whole-sky cameras that are systems that raise increasing attention in the last times

1-General comments

In general, Referee #2 misses more cases of sunphotometer-camera comparison, mainly for partially cloudy and overcast conditions. We agree with this comment, but the comparison between camera and sunphotometer is not trivial when the sky is covered by clouds. First, the AERONET products, such as radiance, have not the enough quality under overcast or partially cloudy conditions. Another problem is the time shift between the sunphotometer measurements and the picture of the camera, because under partially cloudy skies, the clouds position is continuously changing and a cloudless pixel could correspond to a cloudy sunphotometer measurement just a few seconds later. These reasons lead us to use exclusively cloud-free sunphotometer measurements for a radiance comparison with the camera. Regarding the large number of cases on Section 5.2, we have done a global summary about the average radiance for 120 images: 40 cloudless, 40 overcast and 40 partially cloudy:

120 images (40 for each condition) were selected and analyzed for each sky condition. The mean radiance per solid angle and its standard deviation were calculated for each image. The average of the mean radiance and its standard deviation for the 40 cloudless images were 34 (±24), 55 (±29) and 89 (±40) $mWm^{-2}nm^{-1}sr^{-1}$ for the 626, 534 and 464 nm wavelengths, respectively, showing similar results as in the cloudless images of Fig. 6. In the case of overcast skies the average radiance were 63 (±14), 70 (±16) and 80 (±18) $mWm^{-2}nm^{-1}sr^{-1}$ for the red, green and blue channel, respectively. Additionally, 73

(±35), 81 (±29) and 119 (±40) $mWm^{-2}nm^{-1}sr^{-1}$ were the average values of the radiance mean and standard deviation of the 40 partially cloudless images for the 626, 534 and 464 nm wavelengths. These results are in agreement with all conclusions obtained from Fig. 6, where the coefficient of variation increases with the wavelength except for overcast skies when the coefficient of variation is constant and close to 20%.

We will add this analysis (the last paragraph) at the end of section 5.2 in the revised version of the manuscript.

2-Some specific comments

Referee Comment #1: Page 1878, Line 17. Given that only images recorded in 2011 have been used, the details on the degradation of the acrylic dome during 2010 are not relevant, but how the "stability" of the glass dome along 2011 was determined?

Authors response #1: The stability was not checked, but the results in the variation of daily K-matrices (Table 3) are useful to assume a negligible variation in the glass dome properties. The new glass dome presents the same features of the typical sky dome used in pyranometers, that presents negligible degradation when exposed to the environment. On the other hand, acrylic dome presents evidence of the degradation through a reduction of its transparency and the evidence of aging of the outer surface that is scratched by any abrasive material carried out by the wind.

Referee Comment #2: Page 1879, Line 6. Angular distortion of the lens is claimed to be less than 0.8%. How is exactly defined the angular distortion? Have the authors performed any test to determine how this parameter is modified by the glass dome? In other words, how is the mapping of the sky hemisphere over the plane CCD sensor? This mapping would affect the determination of the solid angle to be used in Equation (5).

Authors response #2: lens manufacturer is who guaranties an angular distortion lower than 0.8%. We didn't carry out any test to determinate the effect of glass dome in the image projection supposing no modifications by dome. However, the lens effect in the image was obtained using a ruler in a dome, observing that the variation of zenith angle

is linear with the pixel distance (equidistant projection in the CCD). This process is explained in detail by Cazorla (2010). The mapping affects the determination of solid angle, but it was calculated using the next method:

The coordinates of the principal plane were calibrated as a function of the number of pixel by a simple method, being the maximum absolute error ±5 pixels horizontally and ±1 pixel vertically (Cazorla, 2010). The next equations give the number of pixel (X and Y coordinates) as a function of the angle in the principal plane (θ_{PP}):

$$P_X = -4.69\theta_{PP} + 450.7\,, \tag{1}$$

$$P_Y = -0.246\theta_{PP} + 439.3\,, \tag{2}$$

where P_X and P_Y are the number of pixel in the X and Y coordinates, respectively. The plane perpendicular to the principal plane was calculated and, using these two perpendicular axis, the Cartesian coordinate system was changed to polar obtaining zenith and azimuth coordinates instead X and Y. Finally, the polar coordinates that view each pixel can be calculated using the next equations:

$$\theta = \sqrt{\frac{(P_X - 450.7)^2 + (439.3 - P_Y)^2}{4.69^2 + 0.246^2}}\,, \tag{3}$$

$$\varphi = \arctan\left(\frac{439.3 - P_Y}{P_X - 450.7}\right) - \arctan\left(\frac{0.246}{4.69}\right), \tag{4}$$

where θ is the zenith angle, and φ is the relative azimuth angle with the sun (positive from South to West), both in degrees. Equations (1), (2), (3) and (4) are only valid for the images before 2010 because a displacement were related in the newest images and the geometric equations were corrected with a displacement of +5 and +3 pixels in X and Y, respectively. Finally, the solid angle viewed by each pixel, Ω in sr, was obtained using the next equations:

$$\Omega = \int_{\varphi_1}^{\varphi_2}\int_{\theta_1}^{\theta_2} \sin(\theta)\,d\theta\,d\varphi\,, \tag{5}$$

Assuming:

$$\Omega = \Delta\varphi\Big]_{\varphi_1}^{\varphi_2}\int_{\theta_1}^{\theta_2} \sin(\theta)\,d\theta\,, \tag{6}$$

if Δφ is considered as the arc which cosine is θ and its sine is the width of pixel:

$$\Delta\varphi\Big]_{\varphi_1}^{\varphi_2} = \arctan\left(\frac{1}{\sqrt{4.69^2 + 0.246^2\theta}}\right). \tag{7}$$

Finally, using Eqs. (5), (6) and (7), the solid angle is given by:

$$\Omega = 2\arctan\left(\frac{1}{\sqrt{4.69^2 + 0.246^2\theta}}\right)\sin\left(\frac{\theta\pi}{180}\right)\sin\left(\frac{\pi}{360\sqrt{4.69^2 + 0.246^2}}\right). \quad (8)$$

Referee Comment #3: Page 1887, Line 13. The authors assume that the calibration matrix does not depend on SZA, given that the daily variation (estimated through the coefficient of variation) of the matrix coefficients is small. However, did the authors observe any trend (dependency on SZA) in these coefficients?

Authors response #3: We found a weak increase in the variability of K_{ij} with the increase in SZA. Therefore, we assumed no SZA dependency on the calibration coefficients, which is perfectly reasonable as Table 2 indicates.

Referee Comment #4: Section 3.2. When comparing the radiative model against the sunphotometer measurements, authors give the mean and the median of ARE (absolute relative error) in Figure 3. Why the authors do not give statistics of the differences, that is, not only the absolute differences? This would inform about systematic deviations.

Authors response #4: We agree with the Referee's comment since the bias can be useful to observe systematic deviations. The bias could be included in Fig. 3 (panels c and d), giving a figure like the Fig. I in this report. In order to include the bias in Fig. 5, this figure could be modified, removing the panels g and h (Fig. II), and representing a new Fig. 6 (Fig. III) with the ARE and the bias. Fig I, II and III are included at the end of this report. The scattering angle has been selected instead the azimuth and zenith angles relative to the sun, as Referee #3 claimed.

The mean and median of the bias (relative difference taking into account the sign) for modelled (LibRadtran) and measurements are shown in panels c and d of Fig. I. These values suggest systematic differences between the modelled values (LibRadtran) and the measurements with an underestimation of the model for 677 nm and an overestimation for 441 nm.

This last paragraph could be included in an improved version of the paper at the end of Sect. 3.2.

Moreover, the bias (panels c and d of Fig. III) indicates that the differences between camera and CIMEL radiances are systematic, and that camera overestimates the measurements at 441 nm (almucantar and principal plane) and at 677 nm (principal plane) except for angles near to the sun and it underestimates the radiance measurements at 501 nm (almucantar and principal plane) and at 677 nm (almucantar).

This last paragraph will be included at the end of Sect. 3.2 of the revised manuscript.

Referee Comment #5: In the conclusions, the authors should stress the applicability of the method by other groups with available camera systems, given that only a radiative transfer modelling is needed to obtain the calibration matrix.

Authors response #5: Taking into account the Referee's comment we could change the last sentence of the paper by the next:
"*The authors encourage researchers and groups with available camera system to apply and use the proposed method to obtain sky radiance from sky images, because only a radiative transfer modelling is needed to derive the calibration matrix*."

3-Some technical corrections:

The spelling will be corrected following the revision requested by Referee #2 if the paper is accepted.

4- Figures

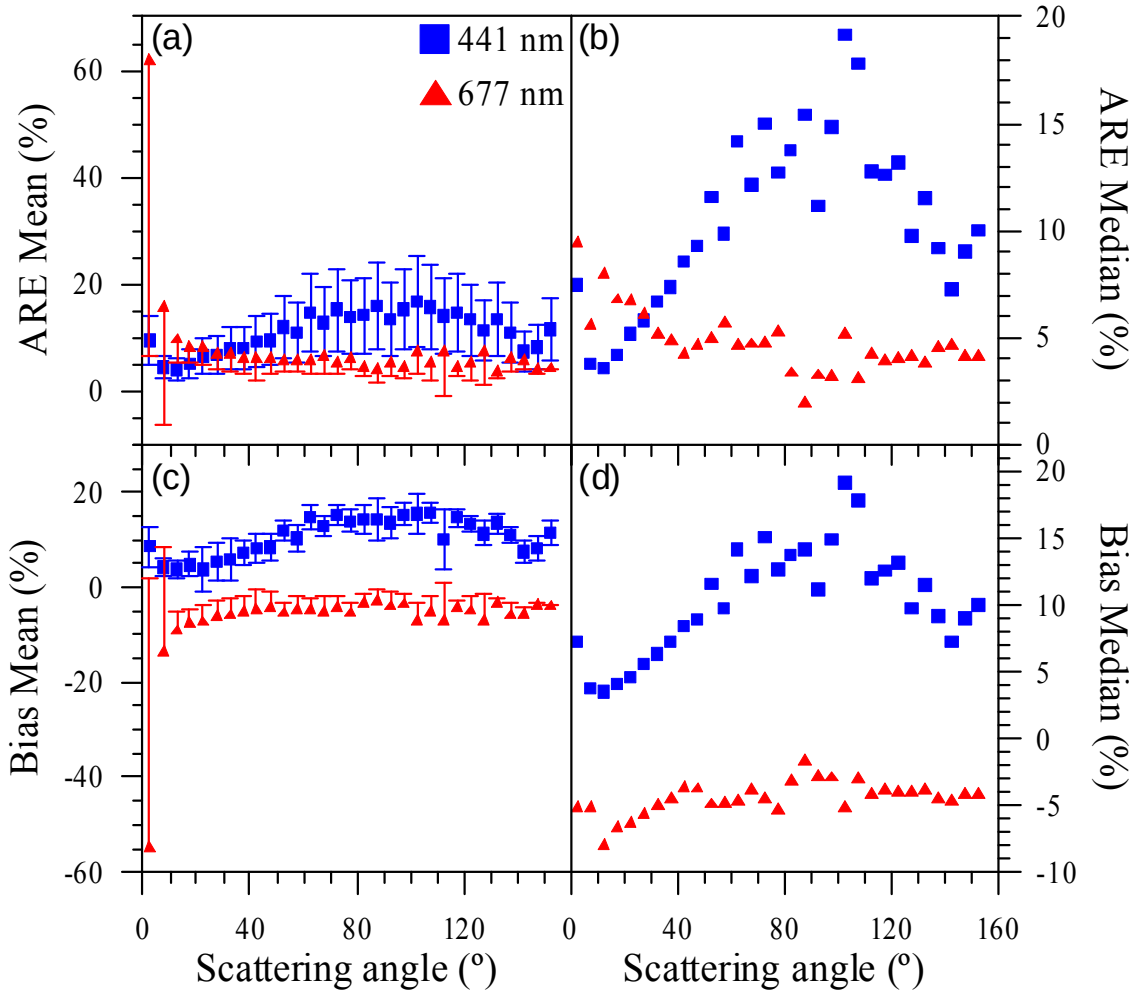

Figure I. Mean (panel a) and median (panel b) of the absolute relative error and bias (panel c and d) for 441 and 677 nm as a function of the scattering angle in the almucantar. The error bars represent the standard deviation, which only the half (up or down) is included for 677 nm due to the high values near to the sun.

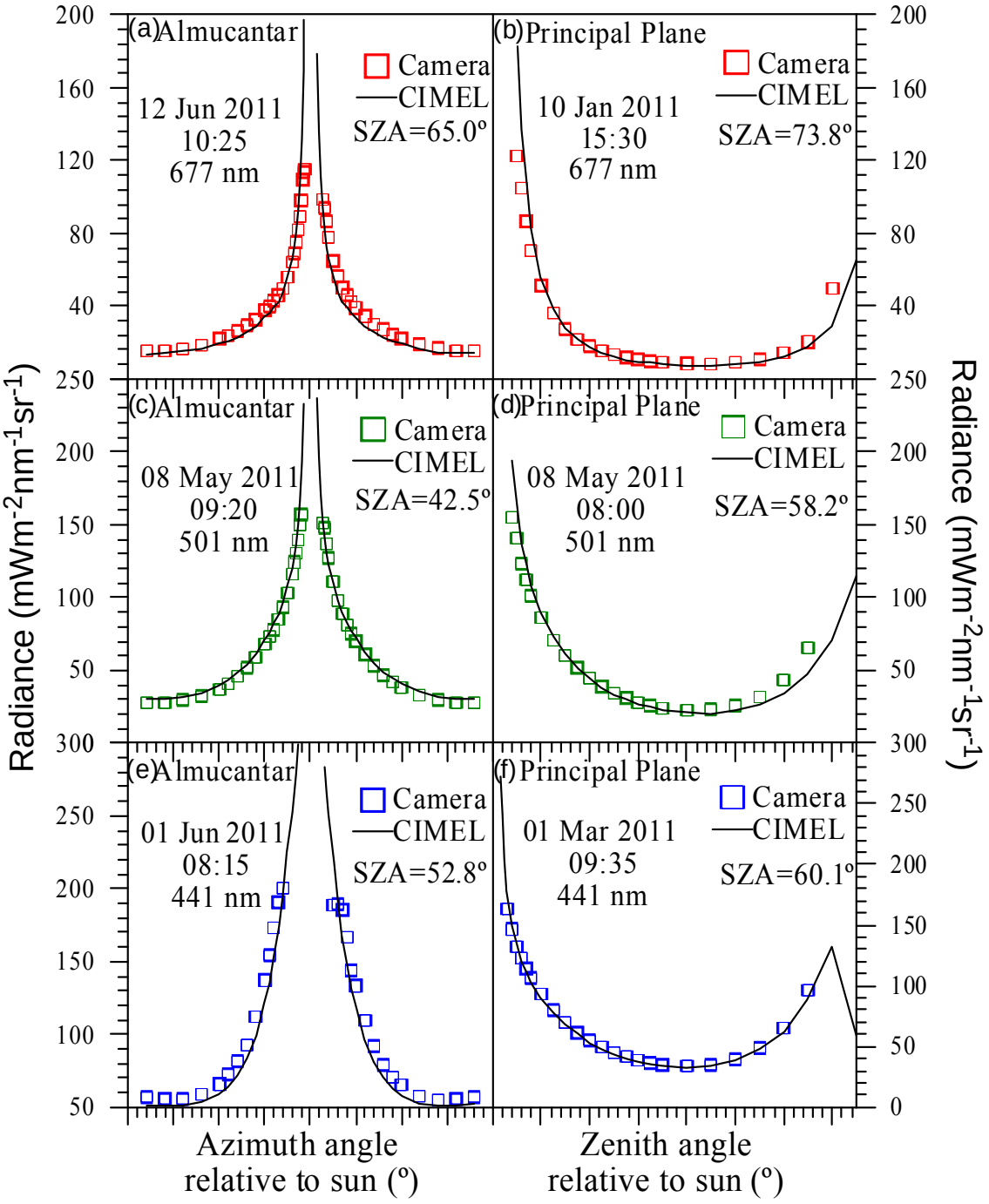

Figure II. The CIMEL and camera sky radiances together for two different dates at 677 nm (panels a and b), 501 nm (panels c and d) and 441 nm (panel e and f). Left panels represent almucantar and right panels are principal planes.

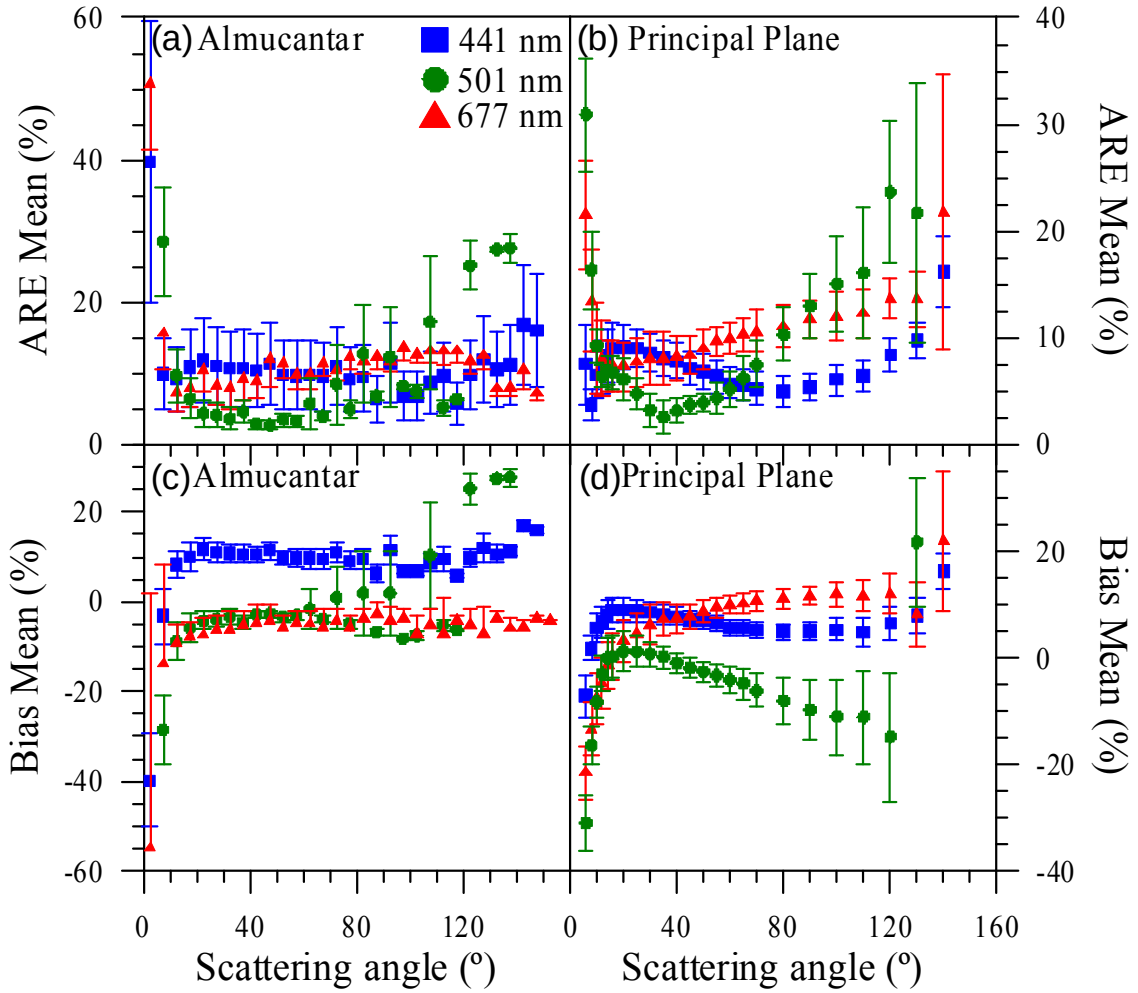

Figure III. Mean of the absolute relative error (panels a and b) and bias (panels c and d) for 677 nm, 501 nm, and 441 nm as a function of the scattering angle. Left panels represent almucantar and right panels are principal planes. The error bars represent the standard deviation, which only the half (up or down) is included for 677 nm (almucantar) due to the high values near to the sun.